Hindawi
Complexity
Volume 2020, Article ID 4764879, 16 pages
https://doi.org/10.1155/2020/4764879

Research Article

A Stabilization Method Based on an Adaptive Feedforward Controller for the Underactuated Bipedal Walking with Variable Step-Length on Compliant Discontinuous Ground

Yang Wang,[1] **Daojin Yao**,[1,2] **Jie He**,[1] **and Xiaohui Xiao**[1]

[1]*Hubei Key Laboratory of Waterjet Theory and New Technology, Wuhan University, Wuhan 430072, China*
[2]*Department of Electrical and Automation Engineering, East China Jiaotong University, Nanchang 330013, China*

Correspondence should be addressed to Xiaohui Xiao; xhxiao@whu.edu.cn

Received 30 July 2019; Revised 4 February 2020; Accepted 6 February 2020; Published 19 March 2020

Academic Editor: Marcin Mrugalski

Both compliance and discontinuity are the common characteristics of the real ground surface. This paper proposes a stabilization method for the underactuated bipedal locomotion on the discontinuous compliant ground. Unlike a totally new control method, the method is actually a high-level control strategy developed based on an existing low-level controller meant for the continuous compliant ground. As a result, although the ground environment is more complex, the calculation cost for the robot walking control system is not increased. With the high-level control strategy, the robot is able to adjust its step-length and velocity simultaneously to stride over the discontinuous areas on the compliant ground surface. The effectiveness of the developed method is validated with a numerical simulation and a physical experiment.

1. Introduction

Underactuated bipedal walking has attracted increasing attention due to the low energy-consumption characteristic [1–4]. In recent years, the research points mainly centralize on mechanism design [5], gait planning [6], motion control [7, 8], and human-machine interaction [9]. However, a real ground surface is of compliance and discontinuity all the time. Because of the difficulty in stabilization control of a periodic system with multisource disturbance, the underactuated bipedal locomotion is still hard to act in real world.

In the early research studies, the ground is assumed to be rigid, and the robot-ground impact is modelled as the rigid body collisions of kinematic chains with an external surface [10, 11]. With this assumption, a nominal gait should be preplanned by considering the actual unevenness of the terrain around the robot, and the bipedal locomotion can be stabilized by finding a control strategy to force each joint position always converging the gait. This method has been used prevalently to realize a stable bipedal locomotion on the rigid uneven ground [12, 13]. However, with the heating up of studying bipedal locomotion on a real pavement, the rigid impact model was no longer capable to be used directly. For example, in a man-made city, to improve the walking comfort and safety, the roads are always paved with large quantities of compliant materials, such as the wood boards and semirigid polyvinyl chloride (PVC) mats which are used commonly in the hospitals, parks, and private houses. As a result, the rigid ground assumption is no longer valid, and the robot-ground impact model is no longer independent of the ground compliance as well [14–18]. In documents, the effect of ground compliance on the bipedal locomotion and the control strategies to cope with it have been studied [19–26].

The ground discontinuity is another obstruction to deploy the underactuated bipedal locomotion in practice. The compliant pavement being crushed and developing into potholes is common due to the inevitable fatigue and corrosion. Because of the difficulty in figuring out the exact conditions in the potholes standing in the way immediately, it is reasonable for the robot to stride over them with adjusted step length. However, the dramatic change of step

length is bound to break the existing periodic stability of the bipedal locomotion system. And the stabilization of an underactuated bipedal locomotion with variable step length is a big challenge. In the literature, Nguyen utilizes a two-step periodic gait optimization technique to build a library of gaits for realizing a variable step-length bipedal walking [27]. Hu et al. used a feedback control method to adjust the robot's step length and walking speed to realize a planar bipedal walking on the uneven ground [28]. Yang et al. applied a reinforcement learning method to supervise the stride-frequency and find out the reasonable step-length online for bipedal walking [29]. However, since these methods are not designed for walking on the compliant ground, they are also incapable of coping with the effects of ground compliance and discontinuity simultaneously.

In this paper, a high-level control strategy is proposed to stabilize an underactuated bipedal walking on the discontinuous compliant ground. The main contribution of this work is the strategy being developed from the features of an adaptive feedforward controller (AFC) which was designed for the locomotion on a continuous compliant ground mentioned in [23] but not from a fresh start. As a result, although the ground environment is much more complex, the calculation cost for the walking system is not increased. The high-level control strategy is composed of a step-length control substrategy and a velocity control substrategy, both of which are developed based on the hysteresis and three monotonicities of the walking system controlled with AFC.

This paper is organized as follows: Section 2 summarizes some conclusions of the AFC method. Section 3 presents the control strategy to stabilize underactuated walking on the discontinuous compliant ground. Section 4 presents the validation of the proposed control strategy, and the conclusions are provided in Section 5.

2. Background

2.1. Adaptive Feedforward Controller. The AFC strategy, inspired by the man's gait characteristic that the walking speed increases when the man's body leans forward and decreases when the body leans back, was proposed to stabilize the underactuated bipedal walking on the compliant ground in our preview work [23]. For brevity, only the principle of AFC is described in this paper.

Firstly, the bipedal locomotion under the effect of ground compliance is modelled as a parameterized single-input-single-output (SISO) system, where the output u_f and the input x_f describe the horizontal velocity and the relative horizontal position of the robot's CoM at the end of each cycle, respectively. And then, a parameter, named as the dissipation ratio and denoted with λ, is used to describe the combined effect of ground compliance and robot's gait on the variation of u_f. When the AFC is working, supposing u_{fd} is the desired value of u_f, λ should be identified online based on the variations of u_f and x_f during the last two walking cycles. And a desired x_{fc} for the current cycle is calculated to control u_f always converging to u_{fd} and thereby keep the robot walking continuous. The schematic of AFC is shown in Figure 1, and only the key equations of [23] are introduced as follows.

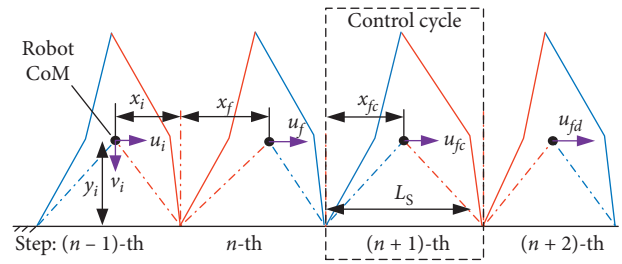

Figure 1: Schematic of AFC.

Based on the SISO model and identified λ, the theoretical value of u_f can be calculated and expressed as

$$u_{f\text{cal}} = U_{\text{rod}}\left(\lambda, v_i, u_i, x_i, x_f, y_i\right), \tag{1}$$

where u and v denote the horizontal and vertical velocities of rod CoM, respectively; x and y are the horizontal and vertical displacements of CoM toward the contact point at the initial time of impact, respectively; and subscripts "i" and "f" denote the initial and final value, respectively.

The calculation of λ is transformed to solving a transcendental equation. Then, by applying the method of 1st-order linearization, λ should be formulated as

$$\begin{aligned}\lambda &= \lambda\left(v_i, u_i, x_i, x_f, y_i, u_f\right)\\ &= \frac{u_f - U_{\text{rod}}\left(0, v_i, u_i, x_i, x_f, y_i\right)}{(\partial/\partial\lambda)U_{\text{rod}}\left(\lambda, v_i, u_i, x_i, x_f, y_i\right)\big|_{\lambda=0}}.\end{aligned} \tag{2}$$

The controlled input x_{fc} can be obtained as

$$\begin{aligned}x_{fc} &= \chi\left(\lambda, v_f, u_f, x_i, y_f, L_S, u_{fd}\right)\\ &= x_f + \frac{u_{fd} - U_{\text{rod}}\left(\lambda, v_f, u_f, x_i, L_S - x_i, y_f\right)}{(\partial/\partial x)U_{\text{rod}}\left(\lambda, v_f, u_f, x, L_S - x_i, y_f\right)\big|_{x=x_i}},\end{aligned} \tag{3}$$

where L_S denotes the step length and subscripts "c" and "d" denote the controlled and desired value, respectively.

2.2. Model of the Ground Discontinuity. Based on the model of the compliant ground established in [23], a discontinuous compliant ground is constructed, as shown in Figure 2. Although the pothole positioning the step-length planning online is already available for a real humanoid robot [30], for simplicity, the position of each pothole is described with the number of steps relative to the origin in this paper. And the width of the largest pothole is not up to 1.5 times longer than the step length of nominal gait.

3. Stabilization Control for Walking on the Discontinuous Compliant Ground

In this section, two features of AFC are studied, and the high-level strategy for stabilizing the walking with variable step length is developed.

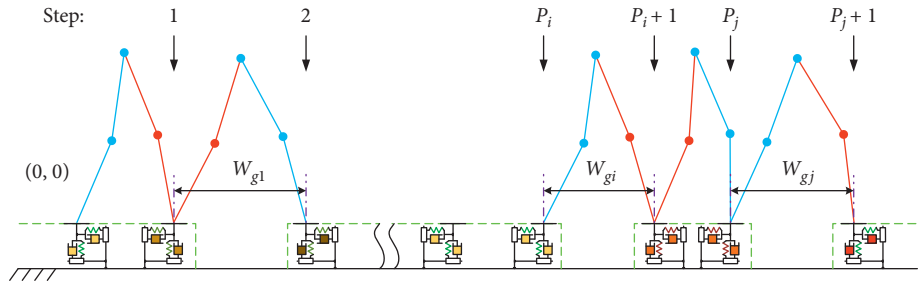

Figure 2: Models of the rigid robot and the compliant ground structure.

3.1. Essentials of the Stabilization Method Development Based on AFC

3.1.1. Hysteresis. Hysteresis is an inherent characteristic for an underactuated bipedal locomotion system controlled with the AFC. According to Section 2.1, the output of AFC is a periodically stable gait meant for a ground with certain compliance. Theoretically, with the gait, periodically stable walking should be realized immediately. However, in practice, the initial state of the robot of each cycle is determined only by the end state of the last cycle. In other words, before a periodically stable state being arrived, the walking system is aperiodic. For example, during this stage, x_{fcn} always equals to x_{fn} but defers from x_{fn-1}. As a result, the ideal effect of AFC is weakened, and the variation of u_{fn} lags behind the variation of u_{fd} in a few cycles. Since the underactuated bipedal locomotion system is an inherent unstable system, this hysteresis would lead to system instability if without any measure.

Fortunately, with the using of λ, the effect of hysteresis is suppressed. And the walking system can be stabilized with AFC even on a ground with variable compliance, as shown in [22]. Thus, to study the hysteresis effect suppression, the relationship between the aperiodicity and the value of λ is studied at first. For brevity, the derivation is detailed in Appendix A, and only conclusions are given as follows.

If $u_{fn} \equiv u_{fd}$ would be realized on a ground with invariant compliance, the following conditions must be satisfied:

$$\begin{cases} \lambda_n > \lambda_{n-1}, & \Delta x > 0, \\ \lambda_n \le \lambda_{n-1}, & \Delta x \le 0, \end{cases} \tag{4}$$

where $\Delta x = x_{in} - x_{idn}$ is the difference between the actual and theoretical initial configurations of the robot of the n-th cycle. According to the inequalities, if the robot's CoM at the initial state is leaning back compared with the previous cycle, the total dissipated kinetic energy of the walking system through this cycle is high than the previous cycle and the walking speed tends to decline and vice versa.

With this conclusion, λ not only quantifies the influence from ground compliance but also reflects the effect of the difference between the actual and theoretical initial configurations of the robot at each cycle. It suppresses the effect of hysteresis of a controlled underactuated bipedal locomotion. This feature is useful to stabilize the walking with variable step length.

3.1.2. Monotonicity. According to the relationship between the three equations introduced in Section 2.1, three monotonicities of AFC are studied and obtained: (1) x_i is inversely proportional to $u_{f\,\mathrm{cal}}$; (2) when x_i is constant, the change of L_S is directly proportional to $u_{f\,\mathrm{cal}}$; and (3) to meet $u_{f\,\mathrm{cal}} = u_{fd}$, the change of x_i is directly proportional to the change of L_S. The derivations of the three monotonicities are detailed in Appendix B.

3.1.3. Deductions for Walking on the Compliance Ground with AFC. When a biped robot, controlled with AFC, walks on a ground with an identical compliance:

(1) λ is reciprocally correlated with L_s. For example, if $L_{sn} < L_{sn-1}, \lambda n > \lambda_{n-1}$ must be satisfied.

(2) x_i is positively correlated with L_s. For example, if $L_{sn} < L_{sn-1}, x_{\mathrm{id}\,n} > x_{in}$ must be satisfied.

(3) u_f is positively correlated with L_s. For example, if $L_{sn} < L_{sn-1}, u_{fcn} < u_{fd}$ must be satisfied.

In summary, the relationship between robot gait and walking speed is shown in Table 1, where "↑" means up, and "↓" means down.

3.2. Strategy for Walking with Variant Step Length.

The bipedal locomotion falling when striding over the pothole shall be attributed to the lack of stall control when only one leg of the biped robot has stepped over the pothole and the other is trying to be recovered, as shown in Table 1. Thus, there are two subobjectives of the control strategy for striding over the potholes and walking stably on the compliant ground:

(1) In the cycle of only one leg stepping over the pothole, u_{fc} should keep the law, the higher the better.

(2) In the cycle after both the legs stepping over the pothole, the decline of u_{fc} must be suppressed.

To meet these objectives, by observing the man's movement when striding over the pothole, a regulatory step with a step length smaller than the nominal should be executed before the robot striding over the pothole to increase u_{fc} sharply, and the desired velocity of the robot's CoM after the both legs have been step over the pothole will change adaptively to suppress the dramatic decreasing of u_{fc}. The control strategy is formulated with two substrategies: step-length control strategy and desired velocity control strategy, as shown in Figure 3.

Table 1: The relationship among x_i, x_{fc}, L_S, u_f, and x_{ic}.

	x_i	x_{fc}	L_S	u_f	x_{ic}
Gait 1	—	↑	—	↑	↓
Gait 2	↓	↑	—	↑	↓
Gait 3	—	—	↑	—	↑

In the step-length control strategy, the designed step length is L_{Sd}, ground discontinuity span is W_g, and the whole walking process includes N cycles. The robot crosses the ground discontinuous area at step i, step i is the span cycle, step $i-1$ is the adjustment cycle, and step $i+1$ is the recovery cycle. Here, the step length of $(i-1)$-th cycle is the difference between two times of the designed step length and the span of ground discontinuity. Therefore, the step-length control strategy is given as follows:

$$\begin{cases} L_{Si} = W_g, \\ L_{S1} = \cdots = L_{Si-2} = L_{Si+1} = \cdots = L_{SN} = L_{Sd}, \\ L_{Si-1} = 2L_{Sd} - L_{Si}. \end{cases} \tag{5}$$

In the desired velocity control strategy, the designed velocity of robot's CoM is u_{fd}, and the change of CoM velocity before and after the adjustment cycle is given as follows:

$$\begin{cases} u_{f1} = \cdots = u_{fd2} = \cdots = u_{fdi} = u_{fdi+3} \cdots = u_{fdn}, \\ u_{fdi+2} = u_{fdi+1} = u_{fi}, \\ u_{fdi+3} = \dfrac{\left(u_{fi+2} + u_{f1}\right)}{2}. \end{cases} \tag{6}$$

In order to prove the effectiveness of the control strategy, theoretical evaluation is given in the Appendix.

4. Experiment and Discussion

4.1. Experimental Setup. A planar point-feet biped robot prototype, UABOT, is shown in Figure 4. UABOT's lateral stabilization is ensured by a directional wheeled cage, and thus, only 2D motion in the sagittal plane is considered. To perform anthropomorphic gaits, UABOT had to have at least a hip and two knees, giving a minimum of four links, where the three joints are actuated. For this external stabilization device not to limit the motion of the robot, including falling down, the cage is only attached to UABOT via a slide-revolute joint system, where the revolute joint is aligned with the axes of the hip, and the sliding joint is along with the normal direction of the ground. In the upright position, with both legs together and straight, the hip is 0.6 m above the ground. UABOT's total mass is 6.5 kg and the cage's 5.8 kg.

To prevent the numerical experiment being diverse from reality, the coefficient of stiffness and damping of real compliant materials to be used in the physical experiment is calculated at first, and the coefficients applied in the numerical experiment should be obtained accordingly.

In the physical experiment, the compliant ground on which UABOT walks is concrete covered with 4 mm poplar particle boards and semirigid PVC mats. According to the elastic modular of the two materials, their equivalent coefficients of stiffness and damping are obtained experimentally, as shown in Table 2. Then, the sets of coefficients of stiffness and damping of the compliant ground to be used in the numerical experiment are determined and shown in Table 3 and Table 4, respectively.

4.2. Numerical Experiment

4.2.1. Effectiveness Evaluation of the Control Strategy for Walking with Variable Step-Length. To evaluate the effectiveness of the control strategy developed for walking with variable step-length, the variations of controlled and uncontrolled u_f when the robot is striding over a pothole are collected. Subject to the geometric constraint of the principle of inverse-kinematics proposed for the gait generation online, the width of the pothole is not larger than 1.5 times the step-length of nominal gait and thus ranges from 0.19 m to 0.27 m. Meanwhile, to suppressing of the effect of ground compliance on the experiment results, a compliant ground with high stiffness and low damping is set, where the coefficients of stiffness and damping are 48×10^4 N/m and 0.01×10^4 N · s/m, respectively. Furthermore, to examine the effectiveness of the whole strategy and the two substrategies, the results with both substrategies simultaneously, only with the step-length control substrategy and velocity control substrategy independently, are shown in Figure 5.

With the step-length control substrategy merely, when $W_g > 0.22$ m, after one leg steps over the pothole, u_f decreases significantly which causes the falling of the walking process. With the velocity control substrategy merely, only when $W_g < 0.27$ m, after one leg steps over the pothole, the other leg is recovered easily and the walking can continue. With the whole strategy, stable walking is realized all the time.

From the above, the necessity of the control strategy is proved which is also in accordance with the result derived in the second half of 2 in Appendix. On the contrary, with the control strategy, u_f is boosted after one leg steps over the pothole which is also in accordance with the proof result of sufficiency discussed in the first half of 2 in Appendix.

4.2.2. Adaptability Evaluation of the Control Strategy for Walking with Variable Step-Length. To evaluate the adaptability of the control strategy, the variation of u_f when

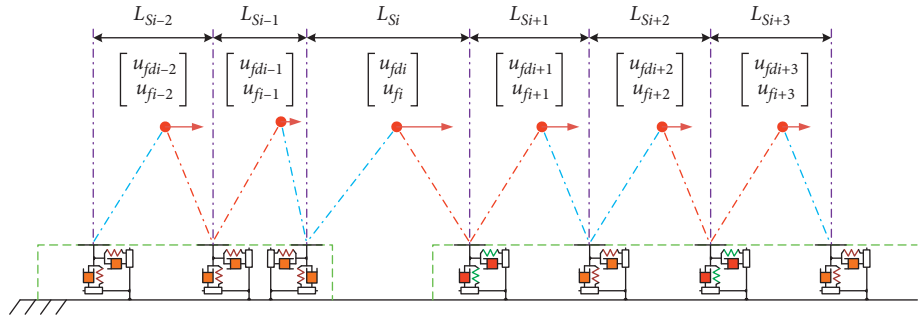

Figure 3: The variable step-length control strategy.

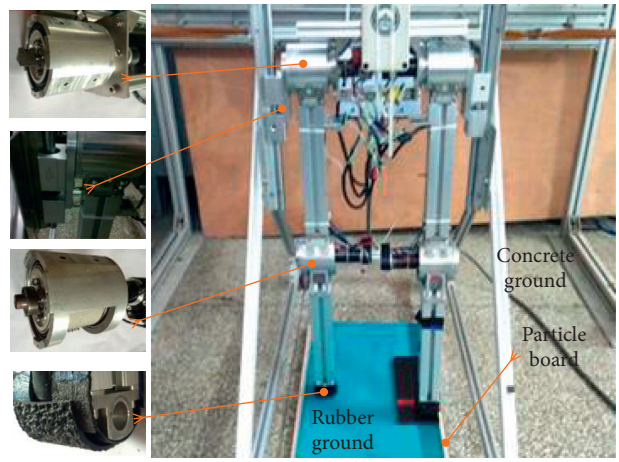

Figure 4: The prototype UABOT.

Table 2: Parameters of 4 mm poplar particle board and semirigid PVC mat.

	Semi-PV	Poplar particle board
Elastic modular	0.39 GPa	2.75 GPa
Equivalent coefficient of stiffness	9.7×10^4 N/m	69×10^4 N/m
Equivalent coefficient of damping	0.0115×104 N·s/m	0.0035×104 N·s/m

Table 3: Set of coefficients of stiffness of the compliant ground ($\times 10^4$ N/m).

k1	k2	k3	k4	k5
3	6	12	24	48

Table 4: Set of coefficients of damping of the compliant ground ($\times 10^4$ N·s/m).

$c1$	$c2$	$c3$	$c4$	$c5$
0.02	0.08	0.32	1.28	5.12

the robot walks on the ground with nonidentical compliance and strides over a series of potholes with different widths is collected. The model of discontinuous compliant ground is built, where the coefficients of stiffness and damping of each compliant unit are selected randomly from Tables 5 and 6, respectively, and the width of each pothole, ranging from 0.19 m to 0.25 m, is also generated randomly, as shown in Tables 5–9.

In Figure 6, the results are shown without and with the controller. With the controller, u_f is always higher than zero, and then, a long-lived bipedal walking is realized even when the ground compliance and the potholes width varying

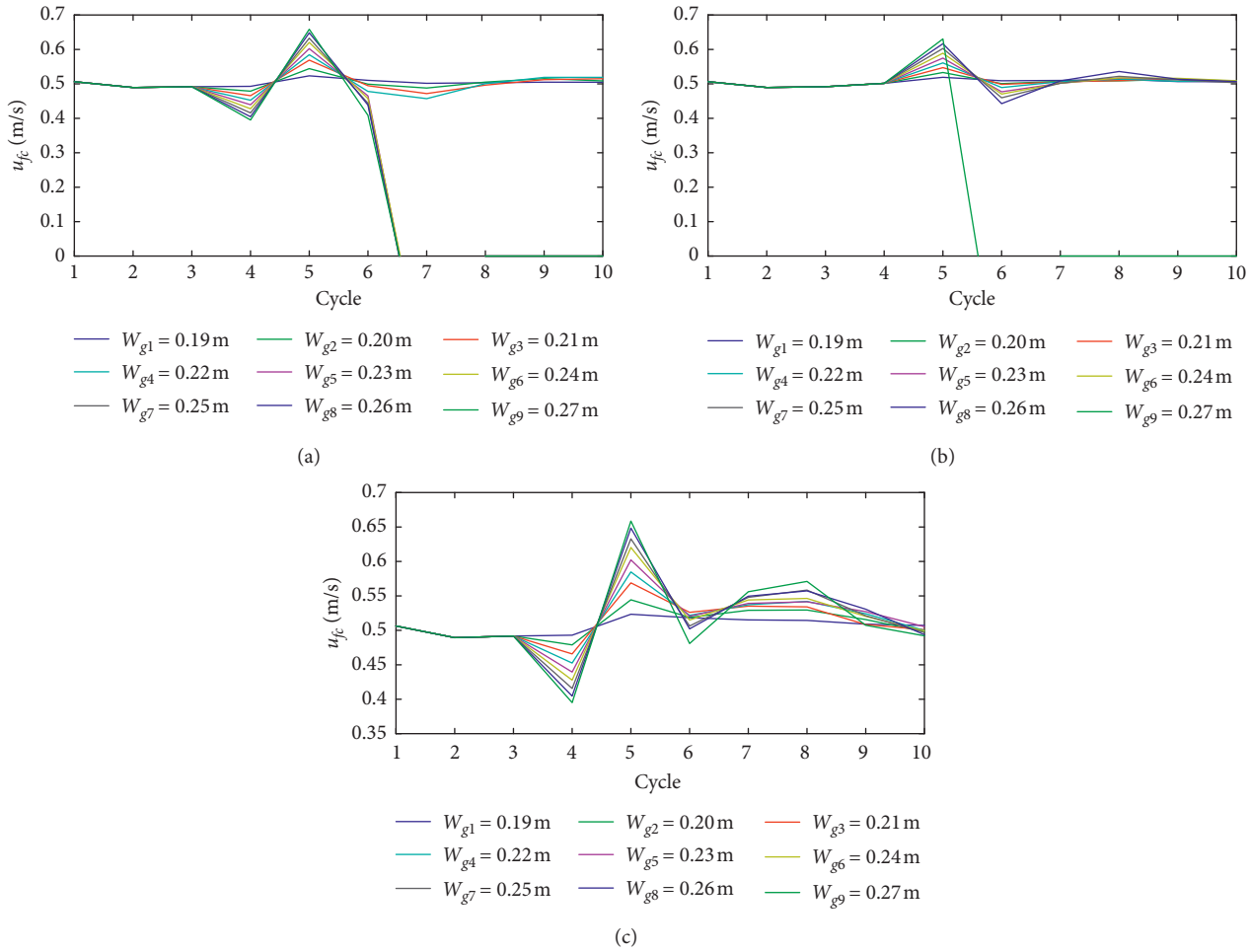

Figure 5: Walking results with different controllers. (a) Step-length control substrategy. (b) Velocity control substrategy. (c) The whole strategy.

Table 5: Distribution of the coefficients of stiffness of the compliant ground.

i	k_i ($\times 10^5$ N/m)	j_i
1	0.7000	1
2	4.7000	2
3	0.3000	8
4	3.8000	11
5	4.0000	14
6	2.2870	19
7	6.0580	33
8	6.0300	41
9	3.0440	45
10	4.5430	51
	Stop	37

Table 6: Distribution of the coefficients of damping of the compliant ground.

i	c_i ($\times 10^5$ N·s/m)	j_i
1	2.8140	1
2	6.6470	2
3	4.6830	5
4	4.3980	8
5	7.3380	9
6	0.9570	24
7	6.0580	11
8	6.0300	14
9	3.0440	17
10	4.5430	20
	Stop	21

simultaneously. From the above, the adaptability of the control strategy in copy with a composite disturbance of the ground environment is demonstrated.

4.3. Physical Experiment. In Figure 7, UABOT is walking on a compliant pavement which is constructed with particle board and semi-PVC mats and striding over a virtual pothole, where $\kappa = 0.32$. Among them, (a)~(c) are the robot's normal gait, (d)~(f) are the adjustment period, (g)~(i) are the span period, (j)~(k) are the recovery period, and (l) is the follow normal gait.

The variations of u_{fc}, v_{sc}, and the configuration of the robot's CoM and step length in the three-time experiments are depicted in Figures 8~10, respectively. GC is representing

Table 7: Series of widths and locations of potholes I.

i	W_{gi} (m)	P_i	i	W_{gi} (m)	P_i
1	0.21	5	5	0.21	24
2	0.20	9	6	0.20	28
3	0.26	14	7	0.26	33
4	0.24	19	8	0.24	37

Table 8: Distribution of the coefficients of damping of the compliant ground.

i	c_i ($\times 10^5$ N·s/m)	j_i
1	5.0870	1
2	7.5620	7
3	1.6730	9
4	5.6750	11
5	1.8910	16
6	0.9570	24
7	4.8590	33
8	3.6020	41
9	3.6710	45
10	5.2960	51
	Stop	37

Table 9: Series of widths and locations of potholes II.

i	W_{gi} (m)	P_i
1	0.21	5
2	0.21	10
3	0.25	14
4	0.23	18
5	0.25	22
6	0.22	27
7	0.21	31
8	0.20	35

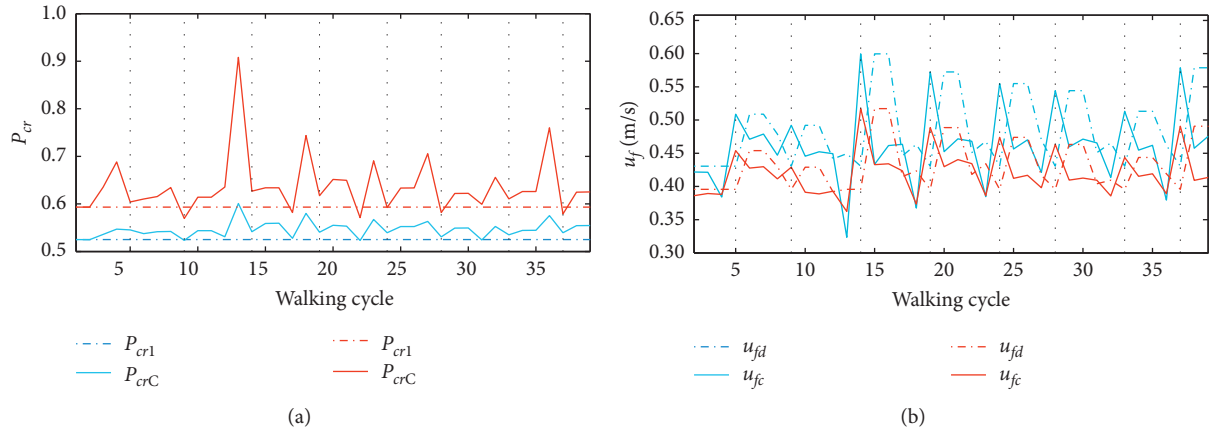

Figure 6: Walking on the discontinuous compliant ground. (a) The relative position changes of the robot CoM. (b) The horizontal velocity changes of the robot CoM.

for the type of ground material, GC is 1 or 2 representing poplar particle board and semirigid, respectively. v_{sci} and u_{fci} represent the corresponding value in the i-th experiment.

With the controller, v_{sc} is always higher than zero, and a long-lived bipedal locomotion is realized. The relationship between the three variables, u_{fc}, x_{fc}, and L_S, is in accordance with the principle of stabilization control strategy developed

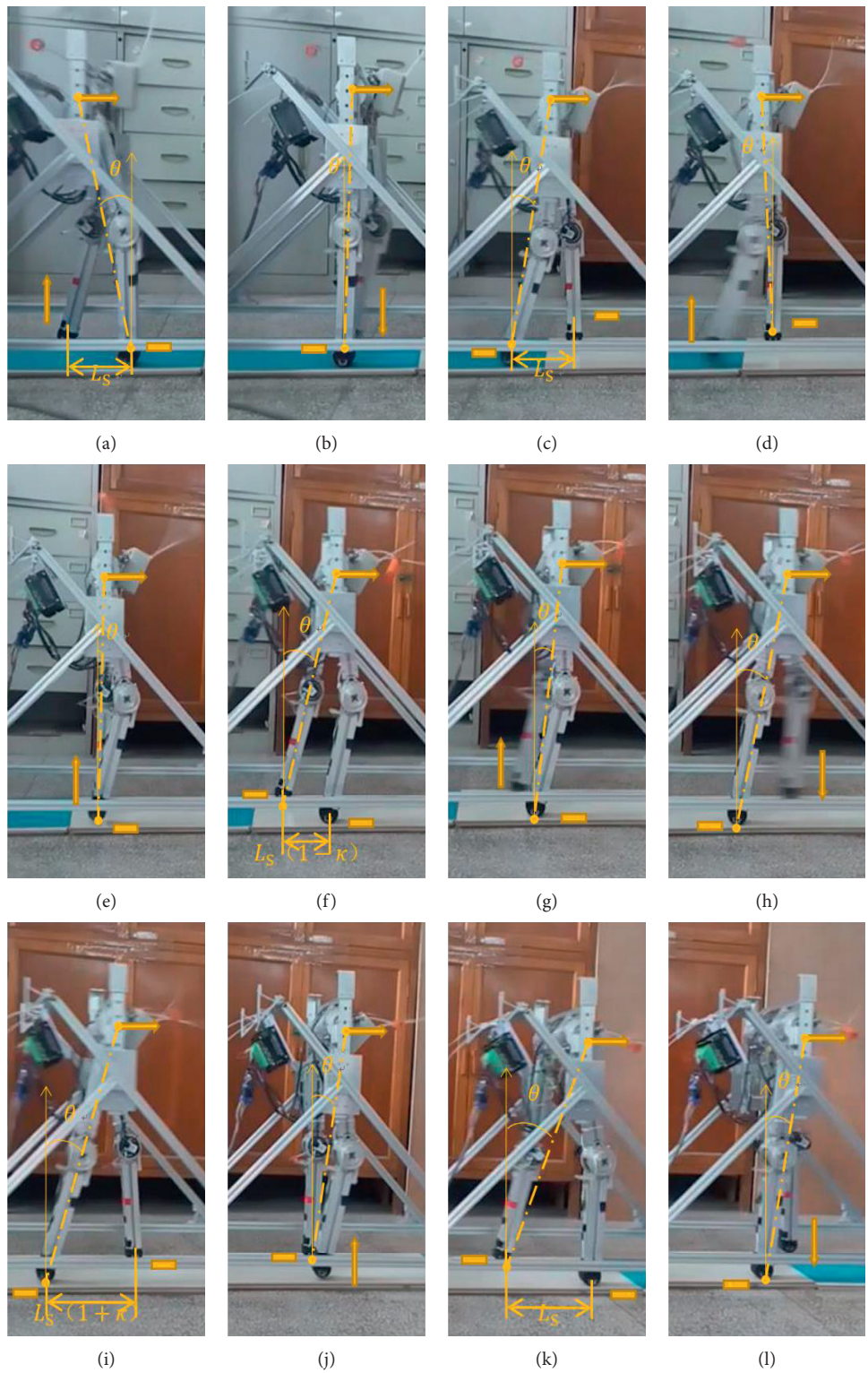

Figure 7: Proceeding of UABOT striding over a pothole where $\kappa = 0.32$ and the compliance of ground is nonidentical ("↓↑": direction of foot movement, "–": sole being in contact with the ground surface, "⟶⟵": direction of hip movement, "NG": nominal gait, SG: gait with short step-length, LG: gait with long step-length, and RG: gait for back leg recovery). (a) Initial stage of NG. (b) SSP of NG. (c) Final state of NG. (d) Initial state of SG. (e) SSP of SG. (f) Final state of SG. (g) Initial state of LG. (h) SSP of LG. (i) Final state of LG. (j) SSP of RG. (k) Final state of RG. (l) SSP of NG.

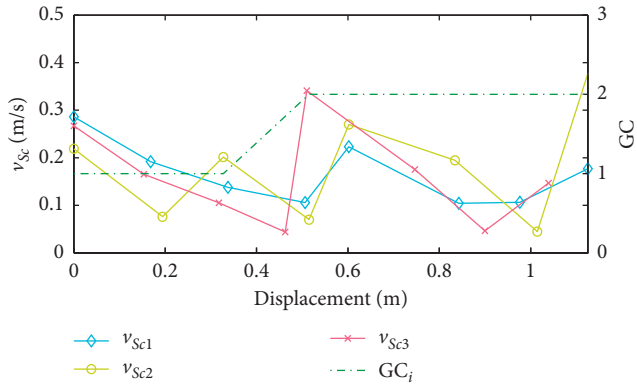

Figure 8: Average speed of each cycle.

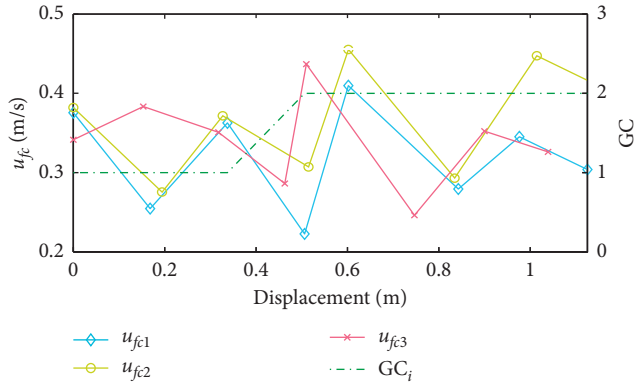

Figure 9: Horizontal velocity of robot's CoM at the end of each DSP.

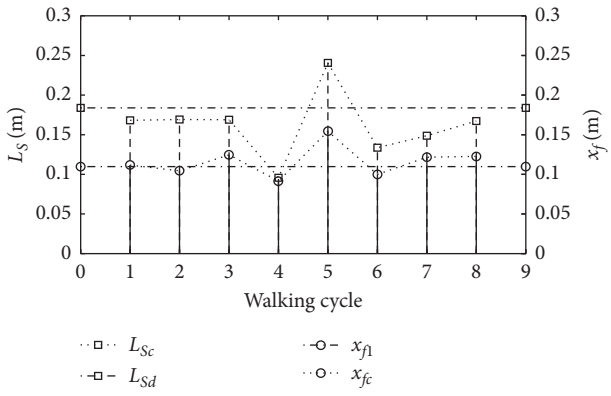

(a)

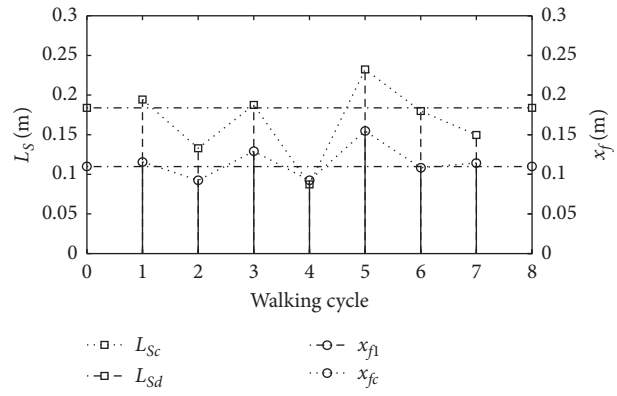

(b)

Figure 10: Continued.

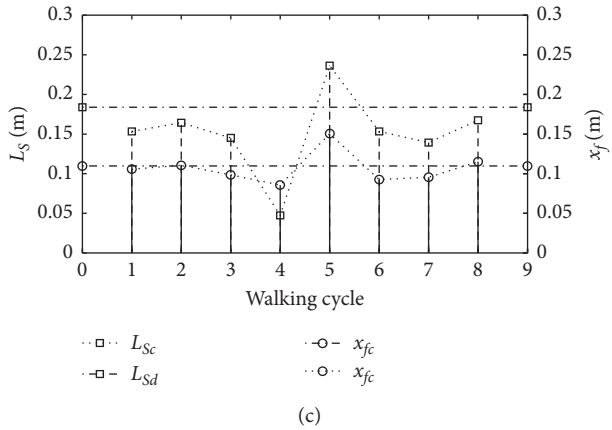

(c)

Figure 10: UABOT's configuration of each cycle in the physical experiment. (a) Variations of x_f and L_s in the 1st experiment. (b) Variations of x_f and L_s in the 2nd experiment. (c) Variations of x_f and L_s in the 3rd experiment.

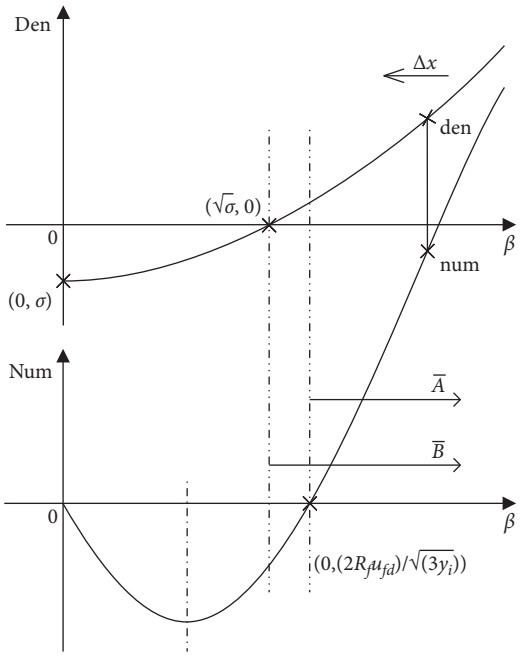

Figure 11: Changes of Num and Den with β.

above. The physical experiment results demonstrate the availability and effectiveness of the control strategy for realizing a bipedal locomotion with variable step length.

5. Conclusions

In this study, a variable step-length control strategy based on an AFC is proposed to stabilize underactuated bipedal walking on the discontinuous compliant ground.

(1) The control strategy achieves a good adaptability to the underactuated bipedal walking system diversity. Since only the robot's CoM state under the ground effect is considered in the controlled input calculation, regardless of the specific ground compliance, robot's structure, and initial gait, the walking process can be stabilized; meanwhile, a desired walking speed can be obtained as well.

(2) The control strategy is low cost and high error tolerance. Since the controlled input is deduced with a polynomial with definite number of degrees, the algorithm is fast and stable, which is beneficial to real-time control. Furthermore, since the joint trajectories' tracking error will be counted in the total effect on the robot's CM motion in the real walking system, the control system has good error tolerance.

(3) The control strategy has broad application prospects. Since the control strategy is essentially originated from the human's gait, it can be integrated into a more advanced bionic control system for bipedal robots to realize a human-like walking in more complicated road environment.

Future work should primarily focus on two issues: (1) how to achieve underactuated bipedal walking on uneven terrains and (2) how to realize 3D bipedal walking.

Appendix

A. Relationship between the Aperiodicity and the Value of λ

Set x_{in} and $x_{\mathrm{id}n}$ which are the actual and ideal initial configurations of the robot at the very beginning of the n-th equivalent cycle, respectively. x_{in} and $x_{\mathrm{id}n}$ must meet the following conditions:

$$\begin{aligned} x_{in} &= L_s - x_{fn-1}, \\ x_{\mathrm{id}n} &= L_s - x_{fcn}, \end{aligned} \tag{A.1}$$

then,

$$x_{in} = \Delta x + x_{\mathrm{id}n}. \tag{A.2}$$

According to (2), by replacing x_{in} with $\Delta x + x_{\mathrm{id}n}$, λ_n is formulated as

$$\lambda_n = \left.\frac{u_{fd} - u_{f\mathrm{cal}\lambda}(\lambda_0)}{\partial u_{f\mathrm{cal}}/\partial\lambda\big|_{\lambda=\lambda_0}}\right|_{\lambda_0=0} = \frac{2\beta^2(\Delta x) - 4R_f u_{fd}/\sqrt{3y_i}\beta(\Delta x)}{\beta^2(\Delta x) - \sigma(\Delta x)} \tag{A.3}$$

where

$$\beta(\Delta x) = \sqrt{g}\sqrt{-(x_{\mathrm{id}n} + \Delta x)^2 + (L_S - x_{\mathrm{id}n})^2 + \frac{Ke_i y_i}{g}},$$

$$\sigma(\Delta x) = Ke_i y_i\left(1 - \frac{2y_i^2 + 2(x_{\mathrm{id}n} + \Delta x)^2}{4y_i^2 + (x_{\mathrm{id}n} + \Delta x)^2}\right),$$

$$Ke_i = u_{in}^2 + v_{in}^2 \quad R_f = \sqrt{x_{fdn}^2 + y_i^2}. \tag{A.4}$$

For $\beta(\Delta x)$ in (A.4), if $\beta(\Delta x) \in R$, the following inequation will be satisfied:

$$\frac{\partial\beta(\Delta x)}{\partial\Delta x} \le 0. \tag{A.5}$$

Then, with the consideration that the robot's CoM is behind the swing foot at the horizontal direction at the very beginning of a DSP, the following inequation will be satisfied:

$$\Delta x + x_{\mathrm{id}n} > 0, \tag{A.6}$$

and then, by differentiating σ with respect to Δx,

$$\frac{\partial\sigma(\Delta x)}{\partial\Delta x} = \frac{12Ke_i y_i^3(x_{\mathrm{id}n} + \Delta x)}{\left(x_{\mathrm{id}n}^2 + 4y_i^2 + 2x\Delta x + \Delta x^2\right)^2}, \tag{A.7}$$

the effective domain of σ and the trend of it over Δx can be obtained:

$$\begin{cases} \sigma(\Delta x) > 0, \\ \dfrac{\partial\sigma(\Delta x)}{\partial\Delta x} > 0. \end{cases} \tag{A.8}$$

Set

$$\mathrm{Num}(\beta) = \frac{2\beta^2(\Delta x) - 4R_f u_{fd}}{\sqrt{3y_i}\beta(\Delta x)},$$

$$\mathrm{Den}(\beta) = \beta^2(\Delta x) - \sigma(\Delta x). \tag{A.9}$$

If $\beta < \beta_0$, where

$$\beta_0 = \frac{R_f u_{fd}}{\sqrt{3y_i}\left(1 + \left(4\sqrt{3}\,Ke_i y^{(5/2)}/g\left(x_{\mathrm{id}n}^2 + 4y_i^2 + 2x\Delta x + \Delta x^2\right)^2\right)\right)} < \frac{2R_f u_{fd}}{\sqrt{3y_i}}, \tag{A.10}$$

the following inequation is satisfied:

$$\frac{\partial\mathrm{Num}(\beta)}{\partial\beta} < \frac{\partial\mathrm{Den}(\beta)}{\partial\beta}. \tag{A.11}$$

The trending of $\lambda(\beta(\Delta x))$ over Δx can be described qualitatively by using a diagram, where only the relative magnitudes of $\mathrm{Num}(\beta)$ and $\mathrm{Den}(\beta)$ are considered, as shown in Figure 11. With the consideration of the sign of λ_{n-1}, the effective domain of $\beta(\Delta x)$ consists of two parts. When $\lambda_{n-1} > 0$, the effective domain of $\beta(\Delta x)$ is described as

$$\begin{cases} \beta \in \overline{A}, \quad \sqrt{\sigma} > \dfrac{2R_f u_{fd}}{\sqrt{3y_i}}, \\ \beta \in \overline{B}, \quad \sqrt{\sigma} < \dfrac{2R_f u_{fd}}{\sqrt{3y_i}}. \end{cases} \tag{A.12}$$

When $\lambda_{n-1} \le 0$, the effective domain of $\beta(\Delta x)$ is described as

$$\beta \in \overline{A} \cap \overline{B}, \tag{A.13}$$

where

$$\overline{A} = \left(\beta \,\middle|\, \frac{2R_f u_{fd}}{\sqrt{3y_i}} < \beta < +\infty\right),$$

$$\overline{B} = (\beta \mid \sqrt{\sigma} < \beta < +\infty). \tag{A.14}$$

According to the above, with the increase of Δx, $\beta(\Delta x)$ is decreased and λ_{n-1} is increased. In other words, if $u_{fn} \equiv u_{fd}$ is to be realized on a certain compliant ground with invariant compliance, the following conditions must be satisfied:

$$\begin{cases} \lambda_n > \lambda_{n-1}, & \Delta x > 0, \\ \lambda_n \le \lambda_{n-1}, & \Delta x \le 0. \end{cases} \tag{A.15}$$

In summary, the AFC can effectively suppress the effect of hysteresis of online identification and the influence of high frequency variation of ground compliance.

B. Monotonicity of AFC

Let x_i, y_i, and L_S satisfy the following relationship:

$$x_i = \varepsilon y_i, \quad \varepsilon \ge 0, \tag{B.1}$$

$$L_S = \eta x_i = \eta\varepsilon y_i, \quad \eta \ge 1, \tag{B.2}$$

where ε and η are two variables. Then, the calculated walking speed $u_{f\mathrm{cal}}$ can be rewritten as

$$u_{f\mathrm{cal}} = \frac{V^\tau y_i}{\sqrt{y_i^2 + (\eta\varepsilon y_i - \varepsilon y_i)^2}}, \tag{B.3}$$

where

$$V^{\tau} = \sqrt{\frac{3}{2} \cdot \frac{Ke_f(\varepsilon) + W_{\gamma}(\varepsilon, \eta)}{m}},$$

$$Ke_f = \frac{1}{2} m\left(u(\varepsilon)^2 + v(\varepsilon)^2 + \rho(\varepsilon)^2 w(\varepsilon)^2\right), \tag{B.4}$$

$$W_{\gamma} = \frac{mg\eta\varepsilon y_i (1-\lambda)(\eta\varepsilon y_i - \varepsilon y_i)}{2y_i}.$$

Then,

$$\frac{\partial u_{f\mathrm{cal}}}{\partial \eta} = -\zeta\varepsilon^2(-1+\eta)\left[mgy_i\left(1+\varepsilon^2\right)(-1+\lambda) + 2Ke_f\right], \tag{B.5}$$

$$\frac{\partial u_{f\mathrm{cal}}}{\partial \varepsilon} = \zeta\Bigg[-2\varepsilon(-1+\eta)^2 Ke_f + y_i\Big(-\varepsilon mg\eta(-2+\eta)(-1+\lambda) + \left(1+\varepsilon^2(1+\eta)^2\right)\frac{\partial Ke_f}{\partial \varepsilon}\Big)\Bigg], \tag{B.6}$$

where

$$\zeta = \frac{1}{2\left[1+\varepsilon^2(1-\eta)^2\right]} \cdot \sqrt{\frac{3}{m\left[1+\varepsilon^2(1-\eta)^2\right]\left[-\varepsilon^2 mg\eta(-2+\eta)(-1+\lambda) + 2Ke_f\right]}}. \tag{B.7}$$

By expending Ke_f and further differentiating it with respect to ε, Ke_f and $(\partial Ke_f/\partial\varepsilon)$ are obtained:

$$Ke_f = \frac{m}{8(4+\varepsilon^2)^4}\left[\phi_1(\lambda)\varepsilon^8 + \cdots + \phi_8(\lambda)\varepsilon + \phi_9(\lambda)\right],$$

$$\frac{\partial Ke_f}{\partial \varepsilon} = -\frac{m}{4(4+\varepsilon^2)^5}\left[\varphi_1(\lambda)\varepsilon^8 + \cdots + \varphi_8(\lambda)\varepsilon + \varphi_9(\lambda)\right]. \tag{B.8}$$

Then,

$$Ke_f \approx \begin{cases} \dfrac{m\left[4u_0^2(2-\lambda)^2 + v_0^2(-4+\lambda)^2\right]}{32}, & \varepsilon \le 1, \\ \dfrac{m\left[u_0^2(-1+\lambda)^2 + v_0^2(1-2\lambda)^2\right]}{2}, & \varepsilon > 1, \end{cases} \tag{B.9}$$

$$\frac{\partial Ke_f}{\partial \varepsilon} \approx \begin{cases} \dfrac{3mu_0v_0(-12+\lambda)\lambda^2}{128}, & \varepsilon \le 1, \\ 0, & \varepsilon > 1. \end{cases} \tag{B.10}$$

By taking (B.15) and (B.16) into (B.7) and (B.8), the following results are obtained:

$$\frac{\partial u_{f\mathrm{cal}}}{\partial \eta} = \begin{cases} -\zeta\varepsilon^2(-1+\eta)\left[mgy(-1+\lambda) + 2Ke_f\right], & \varepsilon \le 1, \\ -\zeta mgy(-1+\lambda)(-1+\eta), & \varepsilon > 1, \end{cases} \tag{B.11}$$

$$\frac{\partial u_{f\mathrm{cal}}}{\partial \varepsilon} = \begin{cases} \dfrac{3}{128}\zeta mu_0v_0y_i(-12+\lambda)\lambda^2, & \varepsilon \le 1, \\ \zeta\varepsilon\left[-2(-1+\eta)^2 Ke_f - gy_i m(-2+\eta)\eta(-1+\lambda)\right], & \varepsilon > 1. \end{cases} \tag{B.12}$$

With the consideration of the definition of λ, the domain of it is

$$|\lambda| \le 1. \tag{B.13}$$

Thus, if $\varepsilon > 1$, the following inequality must be satisfied:

$$\frac{\partial u_{f\mathrm{cal}}}{\partial \eta} > 0. \tag{B.14}$$

While if $\varepsilon \le 1$, the following inequality must be satisfied:

$$\frac{\partial u_{f\mathrm{cal}}}{\partial \varepsilon} \le 0. \tag{B.15}$$

On the contrary, if $\eta < 2$, the following inequality must be satisfied:

$$\zeta\varepsilon\left[-2(-1+\eta)^2 Ke_f - gy_i m(-2+\eta)\eta(-1+\lambda)\right] < 0. \tag{B.16}$$

Furthermore, if (B.1) is solvable in real number field, the following inequality must be satisfied:

$$Ke_f \ge -W_{\gamma}. \tag{B.17}$$

Thus, if $\eta > 1$,

$$2Ke_f \ge mg\varepsilon^2\eta y_i(\eta-1)(-1+\lambda) > mg\eta y_i(-2+\eta)(-1+\lambda) > mg\eta y_i(-1+\lambda), \tag{B.18}$$

is satisfied. Then, if $\varepsilon \le 1$, the following inequality must be satisfied:

$$\frac{\partial u_{f\mathrm{cal}}}{\partial \eta} > 0. \tag{B.19}$$

While, if $\varepsilon > 1$, the following inequality must be satisfied:

$$\frac{\partial u_{f\mathrm{cal}}}{\partial \varepsilon} \leq 0. \tag{B.20}$$

From the above discussion, two conclusions are obtained at first: (1) x_{fc} is positively correlated with $u_{f\,\mathrm{cal}}$ but x_{ic} reciprocally correlated with $u_{f\,\mathrm{cal}}$; (2) L_s is positively correlated with $u_{f\,\mathrm{cal}}$.

Furthermore, with the AFC, the relationship between the three variables, L_{Sd}, x_{ic}, and x_{ic}, can be described as

$$\begin{aligned}\Delta u_{f\mathrm{cal}} &= \frac{\partial u_{f\mathrm{cal}}}{\partial L_{Sd}}\Delta L_{Sd} + \frac{\partial u_{f\mathrm{cal}}}{\partial x_{ic}}\Delta x_{ic} \\ &= \left|\frac{\partial u_{f\mathrm{cal}}}{\partial L_{Sd}}\right|\Delta L_{Sd} - \left|\frac{\partial u_{f\mathrm{cal}}}{\partial x_{ic}}\right|\Delta x_{ic}.\end{aligned} \tag{B.21}$$

Therefore, when $u_{f\,\mathrm{cal}} \equiv u_{fd}$, the following equations

$$\begin{aligned}\left|\frac{\partial u_{f\mathrm{cal}}}{\partial L_{Sd}}\right|\Delta L_{Sd} - \left|\frac{\partial u_{f\mathrm{cal}}}{\partial x_{ic}}\right|\Delta x_{ic} &\equiv 0, \\ \Delta L_{Sd} &= \left|\frac{\partial u_{f\mathrm{cal}}/\partial x_{ic}}{\partial u_{f\mathrm{cal}}/\partial L_{Sd}}\right|\Delta x_{ic},\end{aligned} \tag{B.22}$$

should be satisfied. In other words, to meet $u_{f\,\mathrm{cal}} \equiv u_{fd}$, Δx_{ic} must be always positively correlated with ΔL_{Sd}.

C. Theoretical Evaluation of the Control Strategy

1. Effectiveness Evaluation of Step-Length Control Strategy. Suppose the robot will meet a pothole in the n-th step. According to step-length control strategy and the model of ground discontinuity, the sequence of robot's step length around the pothole can be given as

$$\begin{aligned}L_{Sn} &= (1+\kappa)L_{Sd} = (1+\kappa)\eta_0 x_{in-2}, \\ L_{Sn-1} &= (1-\kappa)L_{Sd} = (1-\kappa)\eta_0 x_{in-2} = \eta_{n-1} x_{in-2},\end{aligned} \tag{C.1}$$

where $\kappa \in (0,1)$.

According to subobjective I, u_{fn} should be increased sharply compared with the nominal value of preplanned gait, u_{f1}. Thus, to evaluate the effectiveness of the step-length control strategy on the increasing of u_f, the walking system is assumed to have been arrived a periodically stable state before the $(n-2)$-th cycle. Some parameters of this stable state can be defined as

$$\begin{aligned}u_{fn-2} &= u_{f1} = u_{fd}, \\ L_{Sd} &= L_{Sn-2} = \eta_0 x_{in-2}, \\ x_{in-2} &= \varepsilon_0 y_i.\end{aligned} \tag{C.2}$$

It must be mentioned that if the bipedal locomotion with invariant step length is periodically stable, the following equation must be satisfied: $u_{in-2} = u_{fn-2} = u_{fd}$. For simplicity, (B.10)–(B.12) are expressed as

$$\begin{aligned}f_\eta^{u_{f\mathrm{cal}}} &= \frac{\partial u_{f\mathrm{cal}}}{\partial \eta}, \\ f_\varepsilon^{u_{f\mathrm{cal}}} &= \frac{\partial u_{f\mathrm{cal}}}{\partial \varepsilon}, \\ f_\varepsilon^{Ke_f} &= \frac{\partial Ke_f}{\partial \varepsilon}.\end{aligned} \tag{C.3}$$

In the $(n-1)$-th walking cycle, if only the step length varying is considered, the theoretical value of u_{fn-1} should be calculated:

$$u_{f\mathrm{cal}\,n-1} = u_{fd} + f_\eta^{u_{f\mathrm{cal}}}(\eta_0)(1-\kappa-1), \quad \eta_0 < u_{fd}. \tag{C.4}$$

Then, to realize $u_{f\,\mathrm{cal}\,n-1} = u_{fd}$, the ideal gait for the $(n-1)$-th cycle will be obtained:

$$\begin{aligned}\varepsilon_{n-1} &= \varepsilon_0 + f_\varepsilon^{u_{f\mathrm{cal}}}(\varepsilon_0)\left(u_{fd} - u_{f\mathrm{cal}\,n-1}\right) \\ &= \varepsilon_0 - f_\varepsilon^{u_{f\mathrm{cal}}}(\varepsilon_0) f_\eta^{u_{f\mathrm{cal}}}(\eta_0)\kappa\eta_0 < \varepsilon_0.\end{aligned} \tag{C.5}$$

Therefore, the total increment of the robot's CoM kinematic energy through the SSP of the $(n-1)$-th can be expressed as

$$W_{\gamma n-1} = \frac{1}{2}mgy_i(1-\lambda_{n-1})\left[\left((1-\kappa)\eta_0\varepsilon_0 - \varepsilon_{n-1}\right)^2 - \varepsilon_0^2\right]. \tag{C.6}$$

The actual value of u_{fn-1} should be calculated theoretically as

$$\begin{aligned}u_{fn-1} &= \sqrt{\frac{3}{2m}\frac{\left(Ke_{fn-2} + W_{\gamma n-1}\right)}{\left[1 + \left((1-\kappa)\eta_0\varepsilon_0 - \varepsilon_0\right)^2\right]}} \\ &= \sqrt{u_{fd}^2 - \Delta\left(u_{fn-1}^2\right)},\end{aligned} \tag{C.7}$$

where

$$\Delta\left(u_{fn-1}^2\right) = \frac{\left(3\Delta W_{\gamma n-1}/2m\right)}{\left[1 + \left((1-\kappa)\eta_0\varepsilon_0 - \varepsilon_0\right)^2\right]}, \tag{C.8}$$

$$\Delta W_{\gamma n-1} = \frac{1}{2}mgy_i(1-\lambda_{n-2})\left(\varepsilon_{n-1}^2 - \varepsilon_0^2\right), \tag{C.9}$$

and the kinematic energy of the robot's CoM at the end the DSP of the $(n-1)$-th walking cycle is calculated as

$$\begin{aligned}Ke_{fn-1} &= Ke_{fn-2} + f_\varepsilon^{Ke_f}(\varepsilon_0)(\varepsilon_{n-1} - \varepsilon_0) \\ &= Ke_{fn-2} - f_\varepsilon^{Ke_f}(\varepsilon_0) f_\varepsilon^{u_{f\mathrm{cal}}}(\varepsilon_0) f_\eta^{u_{f\mathrm{cal}}}(\eta_0)\kappa\eta_0 > Ke_{fn-2}.\end{aligned} \tag{C.10}$$

In the walking n-th cycle, if only the step length varying is considered, the theoretical value of u_{fn} should be calculated:

$$u_{f\mathrm{cal}\,n} = u_{fd} + f_\eta^{u_{f\mathrm{cal}}}(\eta_0)(1+\kappa-1)\eta_0 > u_{fd}. \tag{C.11}$$

Then, to realize $u_{f\mathrm{cal}\,n} = u_{fd}$, the ideal gait for the nth cycle will be obtained:

$$\begin{aligned}\varepsilon_n &= \varepsilon_0 + f_{\varepsilon}^{u_{f\mathrm{cal}}}(\varepsilon_0)\left(u_{fd} - u_{f\mathrm{cal}\,n}\right)\\ &= \varepsilon_0 + f_{\varepsilon}^{u_{f\mathrm{cal}}}(\varepsilon_0) f_{\eta}^{u_{f\mathrm{cal}}}(\eta_0)\kappa\eta_0 > \varepsilon_0.\end{aligned} \tag{C.12}$$

Therefore, the total increment of the robot's CoM kinematic energy through the SSP of the n-th can be expressed as

$$W_{\gamma n} = \frac{1}{2} mg y_i (1 - \lambda_n)\left[\left((1+\kappa)\eta_0\varepsilon_0 - \varepsilon_n\right)^2 - \varepsilon_{n-1}^2\right]. \tag{C.13}$$

The actual value of u_{fn} should be calculated theoretically as

$$\begin{aligned}u_{fn} &= \sqrt{\frac{3}{2m}\frac{\left(Ke_{f\,n-1} + W_{\gamma n}\right)}{\left[1 + \left((1+\kappa)\eta_0\varepsilon_0 - \varepsilon_n\right)^2\right]}}\\ &= \sqrt{u_{fd}^2 + \Delta\left(u_{fn}^2\right)},\end{aligned} \tag{C.14}$$

where

$$\Delta\left(u_{fn}^2\right) = \frac{3}{2m}\frac{\left(\Delta Ke_{fn-1} + \Delta W_{\gamma n}\right)}{\left[1 + \left((1+\kappa)\eta_0\varepsilon_0 - \varepsilon_n\right)^2\right]}, \tag{C.15}$$

$$\Delta Ke_{fn-1} = f_{\varepsilon}^{Ke_f}(\varepsilon_0) f_{\varepsilon}^{u_{f\mathrm{cal}}}(\varepsilon_0) f_{\eta}^{u_{f\mathrm{cal}}}(\eta_0)\kappa\eta_0, \tag{C.16}$$

$$\begin{aligned}\Delta W_{\gamma n} = \frac{1}{2} mg y_i (1 - \lambda_n)\Big(&\left((1+\kappa)\eta_0\varepsilon_0 - \varepsilon_{c\,n}\right)^2 - \varepsilon_{n-1}^2\\ &- \left(\eta_0\varepsilon_0 - \varepsilon_0\right)^2 + \varepsilon_0^2\Big).\end{aligned} \tag{C.17}$$

On the contrary, if the robot is striding over the pothole without the step-length control strategy, the gait of the $(N-1)$-th cycle must be identical to the $(n-2)$-th cycle. Thus, as same as (C.4)~(C.14), in the n-th cycle, the actual value of u_{fn} should be calculated theoretically:

$$W'_{\gamma n} = \frac{1}{2} mg y_i (1 - \lambda'_n)\left[\left((1+\kappa)\eta_0\varepsilon_0 - \varepsilon'_n\right)^2 - \varepsilon_0^2\right], \tag{C.18}$$

$$u'_{fn} = \sqrt{\frac{3}{2m}\frac{\left(Ke_{fn-2} + W'_{\gamma n}\right)}{\left[1 + \left((1+\kappa)\eta_0\varepsilon_0 - \varepsilon'_n\right)^2\right]}} = \sqrt{u_{fd}^2 + \Delta\left(u'^2_{fn}\right)}, \tag{C.19}$$

where

$$\Delta\left(u'^2_{fn}\right) = \frac{3}{2m}\frac{\left(\Delta Ke_{fn} + \Delta W'_{\gamma n}\right)}{\left[1 + \left((1+\kappa)\eta_0\varepsilon_0 - \varepsilon'_n\right)^2\right]},$$

$$\begin{aligned}\Delta W'_{\gamma n} = \frac{1}{2} mg y_i (1 - \lambda'_n)\Big(&\left((1+\kappa)\eta_0\varepsilon_0 - \varepsilon'_n\right)^2 - \varepsilon_0^2\\ &- \left(\eta_0\varepsilon_0 - \varepsilon_0\right)^2 + \varepsilon_0^2\Big).\end{aligned} \tag{C.20}$$

According to (C.10) and (C.18), if $\lambda_n = \lambda'_n$,

$$\varepsilon_{n-1} < \varepsilon_0 \tag{C.21}$$

must be satisfied. Thus,

$$u_{fn} > u'_{fn} \tag{C.22}$$

is satisfied. Furthermore, according to the conclusion of 3.1.1, in the $(n-1)$-th cycle, $\varepsilon_{n-1} < \varepsilon_0$; thus,

$$\lambda_n < \lambda'_n \tag{C.23}$$

must be satisfied. Thus,

$$u_{fn}(\lambda_n) > u'_{fn}(\lambda'_n) \tag{C.24}$$

is satisfied. Since $u_{fn-1} < u_{fd}$ must be satisfied, to realize $u_{f\mathrm{cal}} = u_{fd}$,

$$\varepsilon_n < \varepsilon'_n \tag{C.25}$$

must be satisfied. Thus,

$$u_{fn}(\lambda_n, \varepsilon_n) > u_{fn}(\lambda'_n, \varepsilon'_n) \tag{C.26}$$

must be satisfied. According to the aforementioned, with the step-length control strategy, u_{fn} is increased sharply, and subobjective I is fulfilled.

2. Effectiveness Evaluation of Desired Velocity Control Strategy. The sufficiency of the desired velocity control strategy should be evaluated at first. In the $(n+1)$-th cycle, $L_{S\,n+1} = L_S$. Set $u_{fn}(\lambda_n, \varepsilon_n)$ to be the initial velocity of the robot's CoM at the beginning of the $(n+1)$th equivalent cycle. In consideration of the algorithm of AFC, if $x_{ic\,n+1} = \varepsilon_0 y_i$, $u_{f\mathrm{cal}} = u_{fn}(\lambda_n, \varepsilon_n)$ must be satisfied. Since without the desired velocity control strategy, the control objective should be $u_{fd\,n+1} = u_{f1}$, and the ideal gait of the $(n+1)$-th cycle should be calculated as

$$\varepsilon'_{n+1} = \varepsilon_0 + f_{\varepsilon}^{u_{f\mathrm{cal}}}(\varepsilon_0)\left[u_{fd} - u_{fn}(\lambda_n, \varepsilon_n)\right] > \varepsilon_0. \tag{C.27}$$

The increment of the kinematic energy through the SSP of the $(n+1)$-th cycle should be calculated as

$$W'_{\gamma n+1} = \frac{1}{2} mg y_i (1 - \lambda_{n+1})\left[\left(\eta_0\varepsilon_0 - \varepsilon_{n+1}\right)^2 - \varepsilon_n^2\right]. \tag{C.28}$$

Then, the actual value of u_f in the $(n+1)$-th cycle should be calculated as

$$\begin{aligned}u'_{fn+1} &= \sqrt{\frac{3}{2m}\frac{\left(Ke_{f\,n} + W'_{\gamma n+1}\right)}{\left[1 + \left(\eta_0\varepsilon_0 - \varepsilon_{n+1}\right)^2\right]}}\\ &= \sqrt{u_{fd}^2 - \Delta\left(u_{f\,n+2}^2\right)'},\end{aligned} \tag{C.29}$$

where $Ke_{f\,n}$ is the actual kinematic energy of the robot's CoM at the end of the DSP of the $(n+1)$-th walking cycle and can be expressed as

$$Ke_{fn} = Ke_{fn-2} + f_{\varepsilon}^{Ke_f}(\varepsilon_0)(\varepsilon_n - \varepsilon_0) = Ke_{fn-2} + f_{\varepsilon}^{Ke_f}(\varepsilon_0) f_{\varepsilon}^{u_{f\mathrm{cal}}}(\varepsilon_0) f_{\eta}^{u_{f\mathrm{cal}}}(\eta_0)\kappa\eta_0 < Ke_{fn-2}, \tag{C.30}$$

$$\Delta\left(u_{fn+1}^2\right)' = \frac{3}{2m}\frac{\left(\Delta Ke_{fn} + \Delta' W_{\gamma n+1}\right)}{\left[1 + \left(\eta_0\varepsilon_0 - \varepsilon_{0\,n+1}\right)^2\right]}, \tag{C.31}$$

$$\Delta W'_{\gamma n+1} = \frac{1}{2}mgy_i(1-\lambda_{n+1})\left(\left(\eta_0\varepsilon_0 - \varepsilon_0\right)^2 - \varepsilon_0^2 - \left(\eta_0\varepsilon_0 - \varepsilon'_{n+1}\right)^2 + \varepsilon_n^2\right). \tag{C.32}$$

On the contrary, with the desired velocity control strategy, the actual initial velocity is identical to the desired final state, subject to $\lambda = \lambda_n$, and the ideal gait of the $(n+1)$-th cycle must be obtained as

$$\varepsilon_{n+1} = \varepsilon_0. \tag{C.33}$$

The increment of the kinematic energy through the SSP of the $(n+1)$-th cycle should be calculated as

$$W_{\gamma n+1} = \frac{1}{2}mgy_i(1-\lambda_{n+1})\left[\left(\eta_0\varepsilon_0 - \varepsilon_0\right)^2 - \varepsilon_n^2\right]. \tag{C.34}$$

Then, the actual value of u_f in the $(n+1)$-th cycle should be calculated as

$$u_{fn+1} = \sqrt{\frac{3}{2m}\frac{\left(Ke_{fn} + W_{\gamma n+1}\right)}{\left[1 + \left(\eta_0\varepsilon_0 - \varepsilon_0\right)^2\right]}} = \sqrt{u_{fn}^2 - \Delta\left(u_{fn+1}^2\right)}, \tag{C.35}$$

where

$$\Delta\left(u_{fn+1}^2\right) = \frac{3}{2m}\frac{\left(\Delta Ke_{fn} + \Delta W_{\gamma n+1}\right)}{\left[1 + \left(\eta_0\varepsilon_0 - \varepsilon_0\right)^2\right]}, \tag{C.36}$$

$$\Delta Ke_{fn} = f_{\varepsilon}^{Ke_f}(\varepsilon_0) f_{\varepsilon}^{u_{f\mathrm{cal}}}(\varepsilon_0) f_{\eta}^{u_{f\mathrm{cal}}}(\eta_0)\kappa\eta_0, \tag{C.37}$$

$$\Delta W_{\gamma n+1} = \frac{1}{2}mgy_i(1-\lambda_{n+1})\left(\varepsilon_n^2 - \varepsilon_0^2\right). \tag{C.38}$$

With the comparison between (C.27) and (C.32), the following inequation should be obtained:

$$u_{fn+1} > u'_{fn+1}. \tag{C.39}$$

The sufficiency of the desired velocity control strategy should be evaluated secondly. According to (C.12) and (C.33),

$$u_{fn+1} \approx \sqrt{u_{fd}^2 + \Delta W_{\gamma n} - \Delta W_{\gamma n+1}}, \tag{C.40}$$

should be obtained. Suppose the ground compliance is invariant. When $\kappa \longrightarrow 0$,

$$\lim_{\kappa \longrightarrow 0^+} u_{fn+1} = u_{fd}, \tag{C.41}$$

should be obtained. While $\kappa \longrightarrow 1$ (suppose the size of the pothole is not larger than twice of the nominal step length), it should be obtained as

$$\lim_{\kappa \longrightarrow 1^-} u_{fn+1} = \sqrt{u_{fd}^2 + \Delta}, \tag{C.42}$$

where without considering the varying of λ, Δ should be described as

$$\Delta \approx \frac{1}{2}mgy_i(1-\lambda_{n+2})\left[\left[(1+\kappa)\eta_0\varepsilon_0 - \varepsilon_n\right]^2 - \varepsilon_{n-1}^2 - \left(\eta_0\varepsilon_0 - \varepsilon_0\right)^2 + \varepsilon_0^2\right]. \tag{C.43}$$

The derivative of Δ with respect to κ should be obtained as

$$\frac{\partial\Delta}{\partial\kappa} = mgy_i(1-\lambda_{n+2})\left[(1+\kappa)\eta_0\varepsilon_0 - \varepsilon_n\right]\eta_0\varepsilon_0. \tag{C.44}$$

If and only if $\eta_0 \le (\varepsilon_n/(1+\kappa)\varepsilon_0)$, $(\partial\Delta/\partial\kappa) \le 0$ will be satisfied. Thus, when $\kappa \longrightarrow 1^-$,

$$\lim_{\kappa \longrightarrow 1^-} \Delta \approx \frac{1}{2}mgy_i(1-\lambda_{n+2})\left(\frac{5}{4}\varepsilon_n^2 + \varepsilon_0\varepsilon_n - \varepsilon_{n-1}^2\right), \tag{C.45}$$

will be satisfied. Then, since

$$\varepsilon_n > \varepsilon_0 > \varepsilon_{n-1} \text{ and } \Delta > 0, \tag{C.46}$$

must be satisfied. In consideration of (C.36),

$$u_{fn+1} \ge u_{fd} = u_{f1}, \tag{C.47}$$

must be satisfied.

From the above, although the proof is not strict, it still can be concluded that, with the desired velocity control strategy, the robot's CoM horizontal velocity will be not lower than the norminal value significantly.

Data Availability

The data used to support the findings of this study are available from the corresponding author upon request.

Disclosure

Yang Wang and Daojin Yao are the co-first authors.

Conflicts of Interest

The authors declare that there are no conflicts of interest regarding the publication of this paper.

Acknowledgments

The authors would like to thank those who helped in finishing this paper. This work was supported by the National Natural Science Foundation of China (NSFC, Grant no. 51675385), Youth Project of Jiangxi Education Department (GJJ190357), and the Fundamental Research Funds for the Central Universities (2662019QD002).

References

[1] J. Ramos and S. Kim, "Dynamic locomotion synchronization of bipedal robot and human operator via bilateral feedback teleoperation," *Science Robotics*, vol. 4, no. 35, pp. 1–12, 2019.

[2] J. W. Grizzle, C. Chevallereau, R. W. Sinnet, and A. D. Ames, "Models, feedback control, and open problems of 3D bipedal robotic walking," *Automatica*, vol. 50, no. 8, pp. 1955–1988, 2014.

[3] C.-Y. Chen and P.-H. Huang, "RETRACTED: review of an autonomous humanoid robot and its mechanical control," *Journal of Vibration and Control*, vol. 18, no. 7, pp. 973–982, 2012.

[4] C. Wang, X. Wu, Y. Ma, G. Wu, and Y. Luo, "A flexible lower extremity exoskeleton robot with deep locomotion mode identification," *Complexity*, vol. 2018, Article ID 5712108, 9 pages, 2018.

[5] K. Sreenath, H.-W. Park, I. Poulakakis, and J. W. Grizzle, "A compliant hybrid zero dynamics controller for stable, efficient and fast bipedal walking on MABEL," *The International Journal of Robotics Research*, vol. 30, no. 9, pp. 1170–1193, 2011.

[6] J. Liu and O. Urbann, "Bipedal walking with dynamic balance that involves three-dimensional upper body motion," *Robotics and Autonomous Systems*, vol. 77, pp. 39–54, 2016.

[7] J. W. Grizzle, G. Abba, and F. Plestan, "Asymptotically stable walking for biped robots: analysis via systems with impulse effects," *IEEE Transactions on Automatic Control*, vol. 46, no. 1, pp. 51–64, 2001.

[8] C. Chevallereau, J. W. Grizzle, and C.-L. Shih, "Asymptotically stable walking of a five-link underactuated 3-D bipedal robot," *IEEE Transactions on Robotics*, vol. 25, no. 1, pp. 37–50, 2009.

[9] W. Dong, X. Cheng, T. Xiong, and X. Wang, "Stretchable biopotential electrode with self-similar serpentine structure for continuous, long-term, stable ECG recordings," *Biomedical Microdevices*, vol. 21, no. 1, pp. 1–8, 2019.

[10] T. Wang, C. Chevallereau, and D. Tlalolini, "Stable walking control of a 3D biped robot with foot rotation," *Robotica*, vol. 32, no. 4, pp. 551–570, 2014.

[11] T. Wang, C. Chevallereau, and C. F. Rengifo, "Walking and steering control for a 3D biped robot considering ground contact and stability," *Robotics and Autonomous Systems*, vol. 60, no. 7, pp. 962–977, 2012.

[12] I. R. Manchester, U. Mettin, F. Iida, and R. Tedrake, "Stable dynamic walking over uneven terrain," *The International Journal of Robotics Research*, vol. 30, no. 3, pp. 265–279, 2011.

[13] H.-W. Park, A. Ramezani, and J. W. Grizzle, "A finite-state machine for accommodating unexpected large ground-height variations in bipedal robot walking," *IEEE Transactions on Robotics*, vol. 29, no. 2, pp. 331–345, 2013.

[14] S. H. Hyon, "Compliant terrain adaptation for biped humanoids without measuring ground surface and contact forces," *IEEE Transactions on Robotics*, vol. 25, no. 1, pp. 171–178, 2009.

[15] J. Aguilar and D. I. Goldman, "Robophysical study of jumping dynamics on granular media," *Nature Physics*, vol. 12, no. 3, pp. 278–283, 2016.

[16] M. Romaszko and B. Sapiński, "Stiffness and damping characteristics of MR fluid-based sandwich beams: experimental study," *Journal of Theoretical and Applied Mechanics*, vol. 56, no. 3, pp. 571–583, 2018.

[17] N. Varma, K. G. Jolly, and K. S. Suresh, "A review on numerical models and controllers for biped locomotion over leveled and uneven terrains," *Advances in Robotics Research*, vol. 2, no. 2, pp. 151–159, 2018.

[18] S. D. Gollob, Y. Manian, R. St. Pierre, A. S. Chen, and S. Bergbreiter, "A lightweight, compliant, contact-resistance-based airflow sensor for quadcopter ground effect sensing," in *Proceedings of the 2018 IEEE International Conference on Robotics and Automation (ICRA)*, pp. 7826–7831, Brisbane, Australia, May 2018.

[19] P. Manoonpong, T. Geng, B. Porr, and F. Worgotter, "The run-bot architecture for adaptive, fast, dynamic walking," in *Proceedings of the 2007 IEEE International Symposium on Circuits and Systems*, pp. 1181–1184, New Orleans, LA, USA, May 2007.

[20] E. R. Westervelt, B. Morris, and K. D. Farrell, "Analysis results and tools for the control of planar bipedal gaits using hybrid zero dynamics," *Autonomous Robots*, vol. 23, no. 2, pp. 131–145, 2007.

[21] W. Hou, T. Zhang, Y. Chen, and H. Ma, "Compliant biped walking on uneven terrain with point feet," *International Journal of Advanced Robotic Systems*, vol. 13, no. 2, pp. 51–59, 2016.

[22] M. Khadiv, S. A. A. Moosavian, A. Yousefi-Koma, M. Sadedel, A. Ehsani-Seresht, and S. Mansouri, "Rigid vs compliant contact: an experimental study on biped walking," *Multibody System Dynamics*, vol. 45, no. 4, pp. 379–401, 2019.

[23] Y. Wang, J. Ding, and X. Xiao, "An adaptive feedforward control method for underactuated bipedal walking on the compliant ground," *International Journal of Robotics and Automation*, vol. 32, no. 1, pp. 63–77, 2017.

[24] D. Yao, Y. Wu, Y. Wang, and X. Xiao, "Experimental validation of a control method for underactuated bipedal walking on compliant ground," *International Journal of Robotics and Automation*, vol. 33, no. 5, pp. 1–8, 2018.

[25] Y. Wu, D. Yao, and X. Xiao, "The effects of ground compliance on flexible planar passive biped dynamic walking," *Journal of Mechanical Science and Technology*, vol. 32, no. 4, pp. 1793–1804, 2018.

[26] J. Yu, J. Cao, W.-H. Liao, Y. Chen, J. Lin, and R. Liu, "Multivariate multiscale symbolic entropy analysis of human gait signals," *Entropy*, vol. 19, no. 10, pp. 557–567, 2017.

[27] Q. Nguyen, A. Agrawal, W. Martin, H. Geyer, and K. Sreenath, "Dynamic bipedal locomotion over stochastic discrete terrain," *The International Journal of Robotics Research*, vol. 37, no. 13-14, pp. 1537–1553, 2018.

[28] Y. Hu, G. Yan, and Z. Lin, "Feedback control of planar biped robot with regulable step length and walking speed," *IEEE Transactions on Robotics*, vol. 27, no. 1, pp. 162–169, 2011.

[29] L. Yang, C. M. Chew, A.-N. Poo, and T. Zielinska, "Autonomous stride frequency and step-length adjustment for bipedal walking control," in *Autonomous Robots and Agents*, pp. 189–198, Springer, Berlin, Germany, 2007.

[30] S. Kuindersma, R. Deits, M. Fallon et al., "Optimization-based locomotion planning, estimation, and control design for the atlas humanoid robot," *Autonomous Robots*, vol. 40, no. 3, pp. 429–455, 2016.